


Two-dimensional altermagnets: Superconductivity in a minimal microscopic model

Bjørnulf Brekke , Arne Brataas , and Asle Sudbø

Center for Quantum Spintronics, Department of Physics,
Norwegian University of Science and Technology, NO-7491 Trondheim, Norway

 (Received 15 August 2023; revised 26 October 2023; accepted 27 November 2023; published 14 December 2023)

We propose a minimal toy model for a two-dimensional altermagnet. The model unravels altermagnetic properties at a microscopic level. We find spin-split electron and nondegenerate magnon bands with a d -wave symmetry. We use the model to explore magnon-mediated superconductivity in altermagnets. The dominant superconducting state is spin polarized with a p -wave symmetry. The state adopts its characteristics from the spin-split electron bands. Furthermore, we find that the superconducting critical temperature of altermagnets can be significantly enhanced by tuning the chemical potential.

DOI: [10.1103/PhysRevB.108.224421](https://doi.org/10.1103/PhysRevB.108.224421)

I. INTRODUCTION

Altermagnets constitute a new subclass of magnetic materials [1]. They are defined as compensated collinear magnets with magnetic sublattices related by rotations instead of inversion or translation [2]. The symmetry of altermagnets allows for effects with a potential to rapidly progress the fields of spintronics [3–8], spin caloritronics [9], and superconductivity [10–16]. The most prominent feature of altermagnets is the large momentum-dependent spin-split electron bands [17–25]. Nevertheless, the properties of altermagnets go beyond their characteristic alternating electron bands and include, e.g., chiral magnons [26].

Spin splitting in altermagnets does not rely on a sizable spin-orbit coupling. This allows for a diverse range of potential materials. So far, RuO_2 has been the main focus of attention [27,28], but there are many candidate materials [2,17,20–22,29–34]. These systems are three-dimensional or quasi-two-dimensional. A monolayer altermagnet would be compelling in the rapidly developing field of van der Waals materials and other two-dimensional magnets [35–37]. One route to altermagnetism is an anisotropic ordering of local orbitals [38]. However, the recent large experimental interest and progress has mainly been on materials where the altermagnetic properties rely on the interplay between magnetic and nonmagnetic atoms. This typically calls for more involved unit cells than ferro- and antiferromagnets. Consequently, much of the research on altermagnets carried out so far has been phenomenological [2,39–41], through *ab initio* calculations or experimental work. The microscopic models for studying altermagnets have typically been effective spin-dependent hopping models in momentum space that replicate electron bands with d -wave symmetry. Although useful, these models do not capture the magnetic ordering, and thus, the origin of the altermagnetic properties remains hidden from a microscopic point of view.

The interplay of magnetism and superconductivity has been a fertile playground for intriguing physics [42–45]. The relation between the unconventional spin splitting in altermagnets and unconventional superconductivity is an open

question. This relation is fascinating because La_2CuO_4 , which is a parent compound of high-temperature superconductors [46], is an altermagnet [2,47]. One intriguing direction is how the fluctuations in localized spins can mediate effective electron interactions that, in turn, give rise to superconductivity [48–51].

Here, we propose a two-dimensional minimal model to study altermagnets microscopically. The model sheds light on nonmagnetic sites as a microscopic origin of the unconventional d -wave spin-split bands and nondegenerate magnon modes. We find that the interplay between electrons and magnons gives rise to a spin-polarized p -wave superconducting state, in which the critical temperature is tunable by the chemical potential. For specific values, we find a dramatic increase in the critical temperature analogous to the squeezing enhancement in conventional antiferromagnets [52,53], however, without the need for an uncompensated interface.

II. MODEL

We consider the lattice in Fig. 1. The nonmagnetic lattice belongs to the plane group $p4mm$ (No. 11).

The magnetic plane point group of the crystal has eight symmetries. These are

$$(E|0), (C_{2z}|0), (\sigma_x|0), (\sigma_y|0), \quad (1a)$$

$$(C_{4z}^+|\mathcal{T}), (C_{4z}^-|\mathcal{T}), (\sigma_{xy}|\mathcal{T}), (\sigma_{x\bar{y}}|\mathcal{T}), \quad (1b)$$

where \mathcal{T} is the time-reversal operator. The operations C_{4z}^- and C_{4z}^+ are fourfold clockwise and counterclockwise rotations about the z axis. Furthermore, σ_x , σ_y , σ_{xy} , and $\sigma_{x\bar{y}}$ are mirror operations about the x axis, y axis, and the diagonals. The lattice is centrosymmetric because the twofold rotation C_{2z} acts as inversion symmetry in two dimensions. However, importantly, this inversion symmetry does not relate the two magnetic sublattices. Instead, they are related by the mirror and rotational symmetries in Eq. (1b). Thus, the magnetic crystal classifies as an altermagnet. In Appendix F, we briefly consider an alternative altermagnetic model due to an anisotropic ordering of local orbitals.

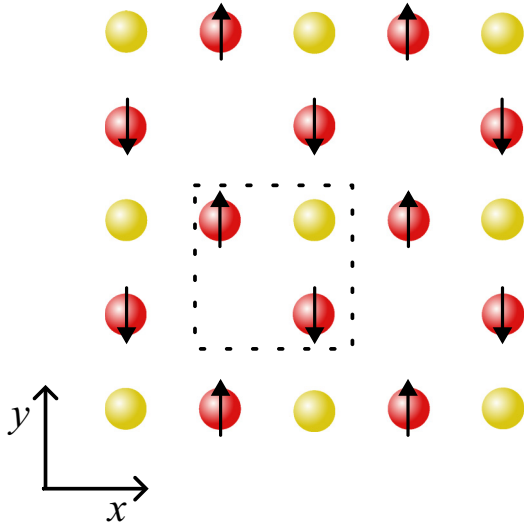


FIG. 1. A two-dimensional alternating magnetic crystal lattice. The unit cell consists of three distinct sites for which rotational symmetries relate the two magnetic sites.

III. ELECTRON PROPERTIES

To study the electron properties, we employ a tight-binding Hamiltonian

$$\begin{aligned}
 H_e = & t \sum_{\langle i,j \rangle, \sigma} c_{i,\sigma}^\dagger c_{j,\sigma} + t_2 \sum_{\langle\langle i,j \rangle\rangle, \sigma} c_{i,\sigma}^\dagger c_{j,\sigma} \\
 & - J_{sd} \sum_{i,\sigma,\sigma'} \mathbf{S}_i \cdot c_{i,\sigma}^\dagger \boldsymbol{\sigma}_{\sigma\sigma'} c_{i,\sigma'} - \mu \sum_{i,\sigma} c_{i,\sigma}^\dagger c_{i,\sigma} \\
 & + \varepsilon_{nm} \sum_{i \in nm, \sigma} c_{i,\sigma}^\dagger c_{i,\sigma},
 \end{aligned} \quad (2)$$

where $c_{i,\sigma}^{(\dagger)}$ is the (creation) annihilation operator of an electron at site i with spin σ . The nearest-neighbor hopping strength is denoted by t . The next-nearest-neighbor hopping strength t_2 governs the hopping between the magnetic sites with opposite magnetization. The chemical potential μ determines the overall doping level, and ε_{nm} is the nonmagnetic site energy. We set the magnetic site energy to zero. The coupling J_{sd} quantifies the on-site exchange interaction between the spin of the itinerant electrons and the localized spins on the magnetic sites \mathbf{S}_i . We emphasize that the model has no spin-orbit coupling term such that the Hamiltonian is block diagonal in spin σ .

We perform a Fourier transform and rewrite the operators in terms of electron band operators $d_{n,\mathbf{k},\sigma} = \sum_{\ell} q_{n,\ell,\mathbf{k},\sigma}^* c_{\ell,\mathbf{k},\sigma}$. Here, ℓ runs over the three sites in the unit cell, n runs over the energy bands, and $q_{n,\ell,\mathbf{k},\sigma}^*$ is chosen such that

$$H_e = \sum_{n,\mathbf{k},\sigma} \varepsilon_{n,\mathbf{k},\sigma} d_{n,\mathbf{k},\sigma}^\dagger d_{n,\mathbf{k},\sigma}. \quad (3)$$

Figure 2 shows the electronic spectrum $\varepsilon_{n,\mathbf{k},\sigma}$ of the minimal model in Eq. (2). The bands exhibit the characteristic spin splitting of altermagnets with a d -wave symmetry. Without next-nearest-neighbor hopping, the model has an accidental particle-hole symmetry relating spin-up and spin-down at half-filling.

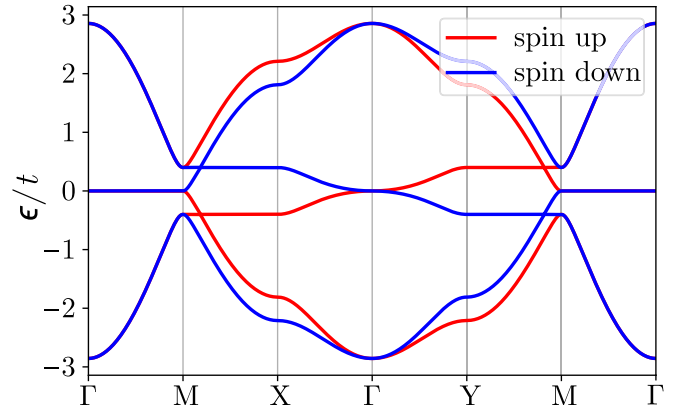


FIG. 2. The electron dispersion in the x and y directions. We used the parameters $t_2/t = 0$, $\mu/t = 0$, $\varepsilon_{nm}/t = 0$, and $J_{sd}S/t = 0.4$.

Figure 3 shows the Fermi surfaces of the electron dispersion in Fig. 2 at four doping levels. The derivation is given in Appendix A. The mirror symmetries of the crystal in Eq. (1b) enforce the electron bands to be spin degenerate along the diagonals $k_x = \pm k_y$. The spin-polarized sectors switch polarity as a function of the chemical potential at $\mu = 0$. The exactness of the switching shown in Fig. 3 is due to an accidental particle-hole symmetry. Nevertheless, the chemical potential μ remains an effective handle for switching the spin polarization even without particle-hole symmetry.

The unconventional spin splitting is consistent with the symmetries in Eq. (1). However, the magnitude of the spin splitting must be determined from microscopic calculations. Figure 4 summarizes how spin splitting depends on the tight-binding parameters in Eq. (2).

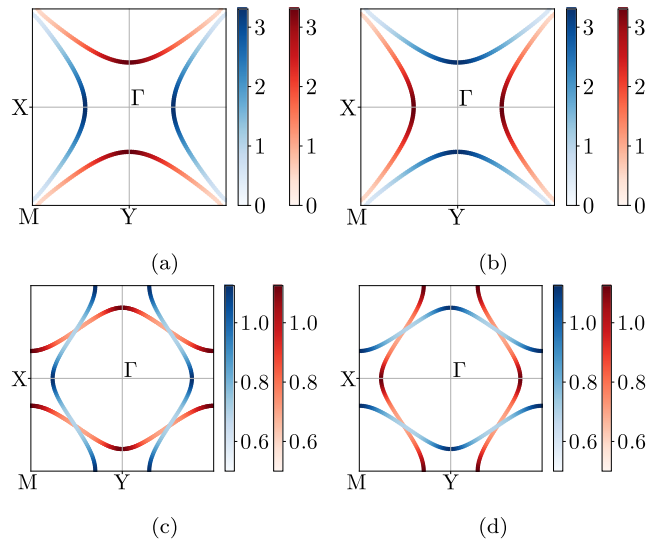


FIG. 3. The Fermi surface at four distinct doping levels. Red and blue correspond to spin-up and spin-down polarization, respectively. The intensity shows the flatness of the bands $|d\varepsilon/dk_{\perp}|^{-1}$, where k_{\perp} is perpendicular to the Fermi surface. The plots are for $J_{sd}S/t = 0.4$, $t_2/t = 0$, $\varepsilon_{nm}/t = 0$ and (a) $\mu/t = 0.1$, (b) $\mu/t = -0.1$, (c) $\mu/t = 2$, and (d) $\mu/t = -2$.

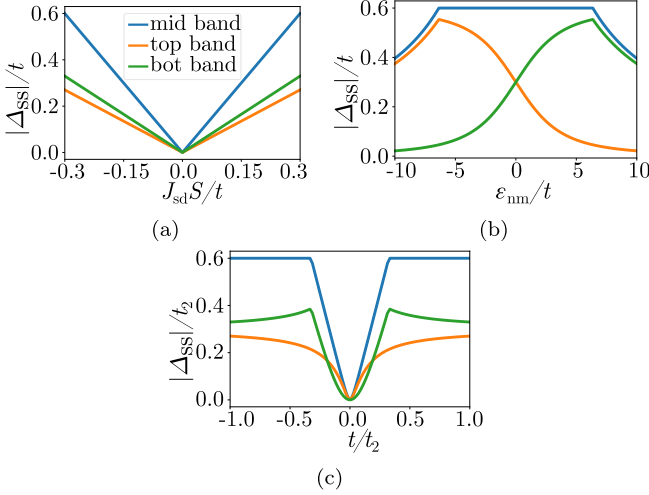


FIG. 4. The magnitude of the maximal spin splitting $|\Delta_{ss}|$ of the three bands as a function of (a) the exchange coupling $J_{sd}S/t$ with $t_2/t = 0$ and $\varepsilon_{nm}/t = 0.4$, (b) the site energy of the nonmagnetic site ε_{nm}/t with $t_2/t = 0$ and $J_{sd}S/t = 0.3$, and (c) the nearest-neighbor hopping t/t_2 with $\varepsilon_{nm}/t_2 = 0.4$ and $J_{sd}S/t_2 = 0.3$.

The spin splitting is directly proportional to the coupling strength $J_{sd}S$. This is generally magnitudes larger than the spin-orbit coupling. Hence, the spin splitting in altermagnets is much larger than spin splitting due to spin-orbit coupling. Figure 4(b) shows that the site energy ε_{nm} of the nonmagnetic site only weakly affects the spin splitting of the middle bands. This illustrates how the presence of the nonmagnetic site, but not necessarily its occupation, is essential for the altermagnetic properties. Figure 4(c) shows the spin splitting as a function of the nearest-neighbor hopping t/t_2 . In the case of $t/t_2 = 0$, the model reduces to that of a conventional antiferromagnet with a nonmagnetic site in the atomic limit. At this point, the spin splitting vanishes due to a restored \mathcal{PT} symmetry.

IV. MAGNON PROPERTIES

Here, we consider the interactions between the localized spins shown in Fig. 1. Nearest-neighbor interactions do not couple the magnetic sublattices. Hence, we consider the effective spin-spin exchange interactions mediated by the nonmagnetic sites, the vacuum sites, and interactions along the diagonals. The inequivalence between the nonmagnetic and empty sites gives rise to an anisotropic exchange interaction with a fourfold symmetry. In other words, the exchange interactions adopt the symmetry of the altermagnet. We consider

$$\begin{aligned}
 H_m = & \sum_{\langle i,j \rangle} J_{AB}(\mathbf{S}_i^A \cdot \mathbf{S}_j^B) + \sum_{\langle i_x, j_x \rangle} (J_{nm} \mathbf{S}_i^A \cdot \mathbf{S}_j^A + J_d \mathbf{S}_i^B \cdot \mathbf{S}_j^B) \\
 & + \sum_{\langle i_y, j_y \rangle} (J_d \mathbf{S}_i^A \cdot \mathbf{S}_j^A + J_{nm} \mathbf{S}_i^B \cdot \mathbf{S}_j^B) \\
 & - \sum_i [K_z (S_{z,i}^A S_{z,i}^A + S_{z,i}^B S_{z,i}^B) + B_z (S_{z,i}^A - S_{z,i}^B)]. \quad (4)
 \end{aligned}$$

Here, the parameters J_{nm} and J_d denote the strength of the exchange interactions mediated by the nonmagnetic sites

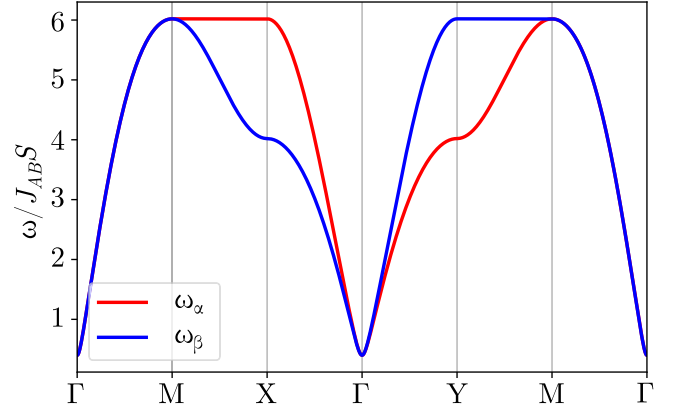


FIG. 5. The magnon dispersion $\omega/J_{AB}S$. Here, we used the parameters $J_{nm}/J_{AB} = -0.5$, $J_d/J_{AB} = 0$, $K_z/J_{AB} = 0.01$, and $B_z = 0$.

and the direct spin exchange between magnetic sites absent an intermediate nonmagnetic site, respectively. These terms couple equal spin sites and are thus ferromagnetic-like. Furthermore, J_{AB} quantifies the interaction strength along the diagonals and couples the magnetic sublattices. It couples sites of opposite spin, giving rise to the antiferromagnetic-like exchange interaction. We also include an easy-axis anisotropy K_z and magnetic field B_z . As outlined in Appendix B, we treat the Hamiltonian to bilinear order in magnon operators by a Holstein-Primakoff transformation and diagonalize it with $a_q = u_q \alpha_q + v_q \beta_{-q}^\dagger$ and $b_{-q}^\dagger = v_q^* \alpha_q + u_q^* \beta_{-q}^\dagger$. Here, $a_q^{(\dagger)}$ and $b_q^{(\dagger)}$ are spin (creation) and annihilation operators at the two magnetic sublattices. The magnon Hamiltonian is then given by

$$H_m = \sum_q [\omega_q^\alpha \alpha_q^\dagger \alpha_q + \omega_q^\beta \beta_q^\dagger \beta_q], \quad (5)$$

where $\alpha_q^{(\dagger)}$ and $\beta_q^{(\dagger)}$ are the (creation) annihilation operators of the magnons with momentum q . The magnon frequencies are $\omega_q^{(\alpha/\beta)} = (-)^+ \gamma_1 + \sqrt{\gamma_2^2 - \gamma_3^2}$ with

$$\gamma_1 = S(J_{nm} - J_d)[\cos(2q_x a) - \cos(2q_y a)] + B_z, \quad (6a)$$

$$\gamma_2 = S(J_{nm} + J_d)[\cos(2q_x a) + \cos(2q_y a)] - 2S(J_{nm} + J_d) + 4SJ_{AB} + 2SK_z, \quad (6b)$$

$$\gamma_3 = 2J_{AB}S[\cos(q_x a + q_y a) + \cos(q_x a - q_y a)]. \quad (6c)$$

The magnon bands in Fig. 5 are split and carry a finite spin expectation value. However, they are not isolated and thus not topological. The mirror symmetry forces band degeneracies along the diagonal without an external magnetic field.

The magnon-band splitting has a d -wave symmetry in momentum space given by

$$\Delta_{\text{magnon}} = 2\{S(J_{nm} - J_d)[\cos(2q_x a) - \cos(2q_y a)] + B_z\}. \quad (7)$$

In other words, the magnon-band splitting arises from inequivalence between the two ferromagnetic-like exchange interaction strengths J_{nm} and J_d .

V. ELECTRON-MAGNON COUPLING

Fluctuations in the localized spins S_i induce an effective electron-magnon coupling from the third term in Eq. (2). We treat this term using the Holstein-Primakoff transformation to second order in magnon operators. The resulting electron-magnon coupling consists of two contributions. The first term is spin-flip processes from first-order magnon operators. This term is generally important for magnon-mediated superconductivity [49,50]. However, for altermagnets, they do not contribute to robust superconducting instabilities.

The second part consists of terms that are second order in magnon operators:

$$H_{\text{em}} = \frac{J_{\text{sd}}}{N} \sum_{k,q,q',\sigma} \left[\sigma M_{q,q'}^B (\Omega_{k+q-q',k,\sigma,\sigma}^B d_{k+q-q',\sigma}^\dagger d_{k,\sigma}) - \sigma M_{q,q'}^A (\Omega_{k+q-q',k,\sigma,\sigma}^A d_{k+q-q',\sigma}^\dagger d_{k,\sigma}) \right]. \quad (8)$$

Here, N is the number of unit cells. We have defined $\Omega_{k',k,\sigma',\sigma}^A \equiv q_{a,k',\sigma'}^* q_{a,k,\sigma}$ and $\Omega_{k',k,\sigma',\sigma}^B \equiv q_{b,k',\sigma'}^* q_{b,k,\sigma}$, where we dropped the band index n because we consider scattering processes on the Fermi surface. The magnon terms are

$$M_{q,q'}^A = u_q^* u_q \alpha_q^\dagger \alpha_q + u_q^* v_q \alpha_q^\dagger \beta_{-q}^\dagger + v_q^* u_q \beta_{-q} \alpha_q + v_q^* v_q \beta_{-q} \beta_{-q}^\dagger, \quad (9a)$$

$$M_{q,q'}^B = v_q^* v_q \alpha_{-q} \alpha_{-q}^\dagger + v_q^* u_q \alpha_{-q} \beta_q + u_q^* v_q \beta_q^\dagger \alpha_{-q}^\dagger + u_q^* u_q \beta_q^\dagger \beta_q. \quad (9b)$$

Based on the electron-magnon coupling, we derive an effective electron-electron interaction using a Schrieffer-Wolff transformation [54]. Finite-momentum Cooper pairs are frail. Hence, we restrict our considerations to interactions between electrons of opposite momenta. Consequently, spin-flip processes associated with the first-order magnon terms are prohibited, except at the spin-degenerate band crossings. These crossings are extremely material dependent and tend to be pointlike at the Fermi surface. We rule them out as secondary effects in the superconducting properties of altermagnets and do not explore this interaction further.

As shown in Appendix D, the spin-conserving scattering processes give rise to an effective electron-electron interaction

$$H_{\text{e-e}} = \sum_{k,k',\sigma} V_{k,k',\sigma} d_{k',\sigma}^\dagger d_{-k',\sigma}^\dagger d_{-k,\sigma} d_{k,\sigma}, \quad (10)$$

where

$$V_{k,k',\sigma} = \frac{-J_{\text{sd}}^2}{N^2} \sum_{\mathcal{Q}} (\Omega_{k',k,\sigma,\sigma}^A |v_{\frac{\mathcal{Q}-(k'-k)}{2}}| |u_{\frac{\mathcal{Q}+(k'-k)}{2}}| - \Omega_{k',k,\sigma,\sigma}^B |v_{\frac{\mathcal{Q}+(k'-k)}{2}}| |u_{\frac{\mathcal{Q}-(k'-k)}{2}}|)^2 \times \left(\omega_{\frac{\mathcal{Q}+(k'-k)}{2}}^\alpha + \omega_{\frac{\mathcal{Q}-(k'-k)}{2}}^\beta \right)^{-1}. \quad (11)$$

Here, we sum over the total magnon momentum $\mathcal{Q} = \mathbf{q} + \mathbf{q}'$. For equal-spin Cooper pairs, the interaction has to be odd in momenta \mathbf{k} and \mathbf{k}' to respect the Pauli principle. We symmetrize the effective interaction and keep the odd contribution.

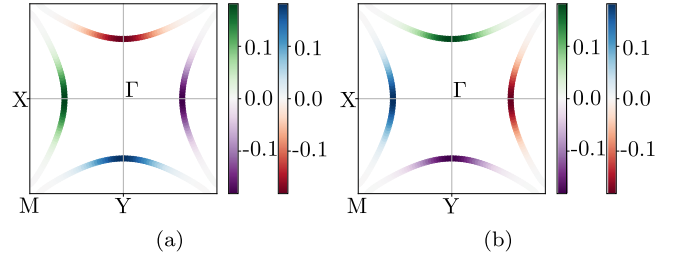


FIG. 6. The superconducting gap profiles of $\Delta_{k,\sigma}$ corresponding to the superconducting state with the critical temperature T_c on the Fermi surface. Red-blue denotes the gap $\Delta_{k,\uparrow}$ and green-purple denotes $\Delta_{k,\downarrow}$. Both gaps are odd in momentum \mathbf{k} and correspond to p -wave superconductivity. The parameters are $J_{\text{sd}}S/t = 0.4$ and (a) $\mu/t = 0.2$, (b) $\mu/t = -0.2$. The magnon dispersion has a smaller energy scale with $J_{AB}S/t = 0.01$. We set $J_{\text{nm}}/J_{AB} = J_{\text{d}}/J_{AB} = -0.5$ and $K_z/J_{AB} = 0.01$.

The superconducting gap is $\Delta_{k,\sigma} = -\sum_{k'} V_{k,k',\sigma} \langle d_{-k',\sigma} d_{k',\sigma} \rangle$, and gives the gap equation

$$\Delta_{k,\sigma} = -\sum_{k'} V_{k,k',\sigma} \frac{\Delta_{k',\sigma}}{E_{k',\sigma}} \tanh\left(\frac{\beta E_{k',\sigma}}{2}\right), \quad (12)$$

with a quasiparticle dispersion $E_{k,\sigma} = \sqrt{\varepsilon_{k,\sigma}^2 + 4|\Delta_{k,\sigma}|^2}$. We linearize the gap equation and perform a Fermi surface average. We take the resulting eigenvalue equation and solve for the largest eigenvalue λ_{eff} . The well-known BCS formula [55] gives the corresponding critical temperature

$$T_c \approx \frac{1.13\omega_M}{k_B} e^{-\frac{1}{\lambda_{\text{eff}}}}. \quad (13)$$

The \mathbf{k} -dependent gap profile $\Delta_{k,\sigma}$ is given by the corresponding eigenvector. Figure 6 shows the gap profile for two distinct values of μ . We note how the doping changes the spin polarization of the bands and serves as a spin switch. The quasiparticle dispersion is fully gapped because the Fermi surface is absent at the nodes. Hence, we expect superconductivity in altermagnets to be robust against weak magnetic and nonmagnetic disorder. For triplet superconductors, the order parameter can be parametrized by the complex \mathbf{d} -vector [56]. It is defined as

$$\hat{\Delta}(\mathbf{k}) = \begin{pmatrix} \Delta_{\uparrow\uparrow}(\mathbf{k}) & \Delta_{\uparrow\downarrow}(\mathbf{k}) \\ \Delta_{\downarrow\uparrow}(\mathbf{k}) & \Delta_{\downarrow\downarrow}(\mathbf{k}) \end{pmatrix} = \begin{pmatrix} -d_x + id_y & d_z \\ d_z & d_x + id_y \end{pmatrix} = i(\mathbf{d}(\mathbf{k}) \cdot \boldsymbol{\sigma})\sigma_y. \quad (14)$$

To parametrize the gap profile in Fig. 6(a), we use two \mathbf{d} -vectors to capture the gap profiles of the disjoint spin-polarized bands. The gap is parametrized by

$$\mathbf{d}_1 = \frac{\Delta(|\mathbf{k}|)}{\sqrt{2}} \text{sgn}(k_x)(-1, i, 0), \quad (15a)$$

$$\mathbf{d}_2 = \frac{\Delta(|\mathbf{k}|)}{\sqrt{2}} \text{sgn}(k_y)(1, i, 0). \quad (15b)$$

Here, the subscripts 1 and 2 correspond to the spin-down and spin-up bands, respectively. The corresponding spin

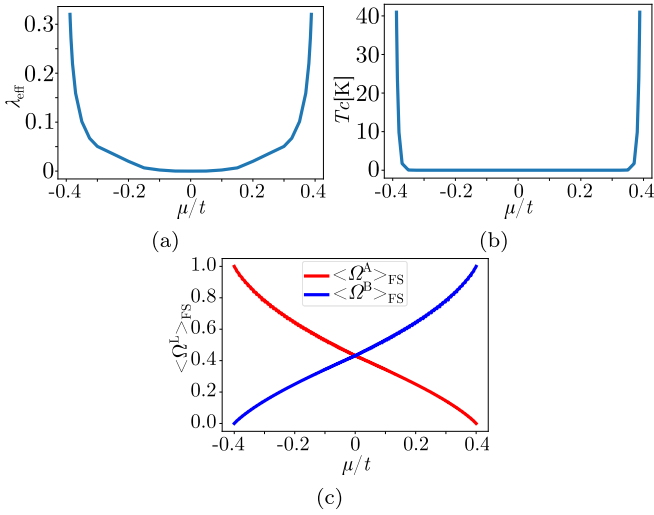


FIG. 7. (a) The interaction strength, (b) critical temperature, and (c) $\langle \Omega_{k,k,\uparrow,\uparrow}^A \rangle_{\text{FS}}$ and $\langle \Omega_{k,k,\uparrow,\uparrow}^B \rangle_{\text{FS}}$ as functions of the chemical potential μ . Here, $J_{\text{sd}}S/t = 0.4$ and $t_2/t = 0$. Furthermore, $J_{AB}S/t = 0.01$, $K_z/J_{AB} = 0.01$, and the magnitude of the localized spins $S = 3/2$. The ferromagnetic-like exchange couplings are $J_{\text{nm}}/J_{AB} = J_A/J_{AB} = -0.5$.

polarizations of the superconducting order parameter for the two bands are

$$\mathbf{q}_1 = i(\mathbf{d}_1 \times \mathbf{d}_1^*) = (0, 0, -|\Delta(|\mathbf{k}|)|^2), \quad (16a)$$

$$\mathbf{q}_2 = i(\mathbf{d}_2 \times \mathbf{d}_2^*) = (0, 0, |\Delta(|\mathbf{k}|)|^2), \quad (16b)$$

consistent with the bands being fully spin polarized.

The estimate of the critical temperature in Eq. (13) is notoriously unreliable due to its exponential sensitivity to material properties. Nevertheless, it could give an idea of the order of magnitude and the qualitative behavior of the superconducting state. Figure 7 highlights the qualitative relation between the occupation of the magnetic sites and the critical temperature T_c . The figure shows a dramatically enhanced critical temperature for certain values of μ . This can be understood as an intrinsic analog to the squeezing effect in Refs. [52,53], without an uncompensated interface.

VI. CONCLUSION

We have introduced a minimal model for altermagnets. The model exhibits the expected behaviors for an altermagnet and

allows for tuning the altermagnetic properties through simple tight-binding parameters. We explore the electron and magnon properties of the model. The electron-magnon coupling gives rise to spin-polarized p -wave superconducting states. Furthermore, we find that the critical temperature can be significantly enhanced by tuning the chemical potential. This effect is an intrinsic analog to the magnon-squeezing effect predicted for antiferromagnets with uncompensated interfaces.

Note added. Recently we found a study that considers a similar magnon model. It considers thermal magnon transport [57].

ACKNOWLEDGMENTS

We thank Kristian Mæland for useful feedback on the manuscript. The Research Council of Norway (RCN) supported this work through its Centres of Excellence funding scheme, Project No. 262633, “QuSpin,” and RCN Project No. 323766.

APPENDIX A: ELECTRON HAMILTONIAN

We consider the altermagnetic square lattice in Fig. 1. The lattice vectors are

$$\mathbf{a}_1 = 2a(1, 0), \quad \mathbf{a}_2 = 2a(0, 1), \quad (A1)$$

where the nearest-neighbor distance $a = 1$. The reciprocal lattice vectors are

$$\mathbf{b}_1 = \frac{\pi}{a}(1, 0), \quad \mathbf{b}_2 = \frac{\pi}{a}(0, 1). \quad (A2)$$

We Fourier-transform the electron operators in Eq. (2) as

$$c_{\ell,i,\sigma} = \frac{1}{\sqrt{N}} \sum_{\mathbf{k}} c_{\ell,k,\sigma} e^{-i\mathbf{k} \cdot \mathbf{r}_i}, \quad (A3)$$

where we assume periodic boundary conditions in both the x and y directions with a total of N unit cells. The crystal momentum \mathbf{k} runs over the first Brillouin zone. The subscript ℓ runs over the three sites in the unit cell $\ell \in (a, \text{nm}, b)$, where a and b refer to the magnetic sites and nm refers to the nonmagnetic site. In this basis, the Hamiltonian is

$$H_e = \sum_{\mathbf{k}, \sigma, \ell, \ell'} c_{\ell,k,\sigma}^\dagger (\mathcal{H}_{\mathbf{k},\sigma})_{\ell,\ell'} c_{\ell',\mathbf{k},\sigma}, \quad (A4)$$

where

$$\mathcal{H}_{\mathbf{k},\sigma} = \begin{pmatrix} -\sigma J_{\text{sd}}S - \mu & 2t \cos k_x a & 2t_2 \cos(k_x a + k_y a) + 2t_2 \cos(k_x a - k_y a) \\ 2t \cos k_x a & -\mu + \varepsilon_{\text{nm}} & 2t \cos k_y a \\ 2t_2 \cos(k_x a + k_y a) + 2t_2 \cos(k_x a - k_y a) & 2t \cos k_y a & \sigma J_{\text{sd}}S - \mu \end{pmatrix}. \quad (A5)$$

We diagonalize this Hamiltonian by introducing the electron band operators

$$d_{n,\mathbf{k},\sigma} = \sum_{\ell} q_{n,\ell,\mathbf{k},\sigma}^* c_{\ell,\mathbf{k},\sigma}, \quad d_{n,\mathbf{k},\sigma}^\dagger = \sum_{\ell} q_{n,\ell,\mathbf{k},\sigma} c_{\ell,\mathbf{k},\sigma}^\dagger. \quad (A6)$$

The diagonal form of the electron Hamiltonian is given in Eq. (3).

1. The Fermi surface

The electron band energies in Eq. (3) are solutions to the secular equation

$$x_0 + x_1\varepsilon + x_2\varepsilon^2 + \varepsilon^3 = 0, \quad (\text{A7})$$

where the coefficients are

$$\begin{aligned} x_0 = & \mu^3 - \mu J_{\text{sd}}^2 S^2 - \mu^2 \varepsilon_{\text{nm}} + J_{\text{sd}}^2 S^2 \varepsilon_{\text{nm}} - 4\mu t^2 - 8t^2 t_2 + 4(-\mu + \varepsilon_{\text{nm}})t_2^2 \\ & + 2[(-\mu - \sigma J_{\text{sd}} S)t^2 - 4t^2 t_2 + 2(-\mu + \varepsilon_{\text{nm}})t_2^2] \cos(2k_y a) + 2 \cos(2k_x a) \{(-\mu + \sigma J_{\text{sd}} S)t^2 - 4t^2 t_2 + 2(-\mu + \varepsilon_{\text{nm}})t_2^2 \\ & + 2t_2[-2t^2 + (-\mu + \varepsilon_{\text{nm}})t_2] \cos(2k_y a)\}, \end{aligned} \quad (\text{A8a})$$

$$\begin{aligned} x_1 = & 3\mu^2 - J_{\text{sd}}^2 S^2 - 2\mu \varepsilon_{\text{nm}} - 4(t^2 + t_2^2) - 2t^2 \cos(2k_x a) - 4t_2^2 \cos(2k_x a) - 2t_2^2 \cos(2k_x a - 2k_y a) \\ & - 2t^2 \cos(2k_y a) - 4t_2^2 \cos(2k_y a) - 2t_2^2 \cos(2k_x a + 2k_y a), \end{aligned} \quad (\text{A8b})$$

$$x_2 = 3\mu - \varepsilon_{\text{nm}}. \quad (\text{A8c})$$

The Fermi surface is the contour defined by $\varepsilon = 0$ such that Eq. (A7) reduces to $x_0 = 0$. We solve for k_x and k_y explicitly to find

$$k_y = \frac{1}{2a} \arccos\left(\frac{-\alpha - \gamma \cos(2k_x a)}{\beta + \delta \cos(2k_x a)}\right) \quad (\text{A9a})$$

and conversely

$$k_x = \frac{1}{2a} \arccos\left(\frac{-\alpha - \beta \cos(2k_y a)}{\gamma + \delta \cos(2k_y a)}\right). \quad (\text{A9b})$$

Here,

$$\alpha = \mu^3 - \mu J_{\text{sd}}^2 S^2 - \mu^2 \varepsilon_{\text{nm}} + J_{\text{sd}}^2 S^2 \varepsilon_{\text{nm}} - 4\mu t^2 - 8t^2 t_2 + 4(-\mu + \varepsilon_{\text{nm}})t_2^2, \quad (\text{A10a})$$

$$\beta = 2[(-\mu - \sigma J_{\text{sd}} S)t^2 - 4t^2 t_2 + 2(-\mu + \varepsilon_{\text{nm}})t_2^2], \quad (\text{A10b})$$

$$\gamma = 2[(-\mu + \sigma J_{\text{sd}} S)t^2 - 4t^2 t_2 + 2(-\mu + \varepsilon_{\text{nm}})t_2^2], \quad (\text{A10c})$$

$$\delta = 4t_2[-2t^2 + (-\mu + \varepsilon_{\text{nm}})t_2]. \quad (\text{A10d})$$

2. Sample the Fermi surface

We solve the superconducting gap equation (12) by employing a Fermi surface average. This requires a uniform sampling of the Fermi surface. To that end, we parametrize the Fermi surface in Eq. (A9a) as

$$k_x = t, \quad k_y = \frac{1}{2a} \arccos\left(\frac{-\alpha - \gamma \cos(2ta)}{\beta + \delta \cos(2ta)}\right), \quad (\text{A11})$$

where $t \in [-\pi/2a, \pi/2a]$. For a fixed segment Δt along the k_x axis, the corresponding segment along the Fermi surface is

$$\Delta s = \Delta t \sqrt{\left(\frac{dk_x}{dt}\right)^2 + \left(\frac{dk_y}{dt}\right)^2}, \quad (\text{A12})$$

where

$$\frac{dk_y}{dt} = -\frac{1}{\sqrt{1 - \left(\frac{\alpha + \gamma \cos(2ta)}{\beta + \delta \cos(2ta)}\right)^2}} \frac{(\gamma\beta - \delta\alpha) \sin(2ta)}{[\beta + \delta \cos(2ta)]^2}. \quad (\text{A13})$$

Now, setting Δs constant and sample Eq. (A11) at intervals

$$\Delta t = \frac{\Delta s}{\sqrt{1 + \left(\frac{dk_y}{dt}\right)^2}} \quad (\text{A14})$$

gives a uniform distribution along the Fermi surface.

APPENDIX B: MAGNON HAMILTONIAN

We consider the Hamiltonian in Eq. (4) and rewrite the spin operators as

$$S_i^{A,x} = \frac{1}{2}(S_i^{A,+} + S_i^{A,-}), \quad S_i^{A,y} = \frac{1}{2i}(S_i^{A,+} - S_i^{A,-}), \quad (\text{B1a})$$

$$S_j^{B,x} = \frac{1}{2}(S_j^{B,+} + S_j^{B,-}), \quad S_j^{B,y} = \frac{1}{2i}(S_j^{B,+} - S_j^{B,-}). \quad (\text{B1b})$$

Then, we quantize the spin operators to linear order using

$$S_i^{A,+} = \sqrt{2S}a_i, \quad S_j^{B,+} = \sqrt{2S}b_j^\dagger, \quad (\text{B2a})$$

$$S_i^{A,-} = \sqrt{2S}a_i^\dagger, \quad S_j^{B,-} = \sqrt{2S}b_j, \quad (\text{B2b})$$

$$S_i^{A,z} = (S - a_i^\dagger a_i), \quad S_j^{B,z} = (-S + b_j^\dagger b_j), \quad (\text{B2c})$$

where S is the magnitude of the localized spins. To diagonalize the Hamiltonian, we use the Fourier transform

$$a_i = \frac{1}{\sqrt{N}} \sum_q a_q e^{-iq \cdot r_i}, \quad (\text{B3})$$

with the same convention for the b operator. We use the Holstein-Primakoff transformation and subsequent Fourier

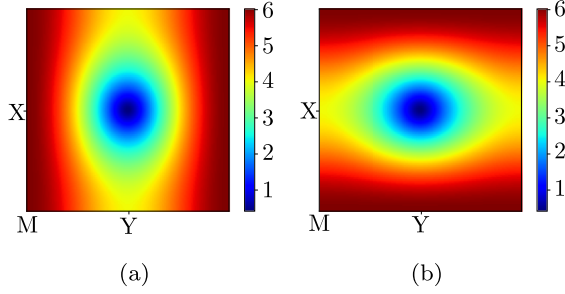


FIG. 8. The magnon modes with $J_{nm}/J_{AB} = -0.5$, $J_d/J_{AB} = 0$, and $K_z/J_d = 0.01$. Here, (a) shows $\omega_q^\alpha/J_{AB}S$ and (b) shows $\omega_q^\beta/J_{AB}S$.

transform to find

$$\begin{aligned}
 H_m = & \sum_q \{S[2J_{nm} \cos(2q_x a) + 2J_d \cos(2q_y a) \\
 & - 2(J_d + J_{nm})] + 4SJ_{AB} + 2SK_z + B_z\} a_q^\dagger a_q \\
 & + \{S[2J_{nm} \cos(2q_y a) + 2J_d \cos(2q_x a) - 2(J_d + J_{nm})] \\
 & + 4SJ_{AB} + 2SK_z - B_z\} b_q^\dagger b_q \\
 & + \{2J_{AB}S[\cos(q_x a + q_y a) + \cos(q_x a - q_y a)]\} a_q b_{-q} \\
 & + \{2J_{AB}S[\cos(q_x a + q_y a) + \cos(q_x a - q_y a)]\} a_q^\dagger b_{-q}^\dagger. \quad (B4)
 \end{aligned}$$

In a matrix form, the Hamiltonian is

$$H_m = \sum_q \begin{pmatrix} a_q^\dagger & b_{-q} \end{pmatrix} \begin{pmatrix} A(q) & B(q) \\ B(q) & C(q) \end{pmatrix} \begin{pmatrix} a_q \\ b_{-q}^\dagger \end{pmatrix}, \quad (B5)$$

where A, B, C can be read off from Eq. (B4). We diagonalize the Hamiltonian by introducing the Bogoliubov

transformation

$$\begin{pmatrix} a_q \\ b_{-q}^\dagger \end{pmatrix} = \begin{pmatrix} u_q & v_q \\ v_q^* & u_q^* \end{pmatrix} \begin{pmatrix} \alpha_q \\ \beta_{-q}^\dagger \end{pmatrix}. \quad (B6)$$

The transformation must respect bosonic commutation relations, which leads to the constraint

$$|u_q|^2 - |v_q|^2 = 1. \quad (B7)$$

We choose

$$u_q = \frac{i}{\sqrt{2}} \sqrt{\frac{A+C}{\sqrt{(A+C)^2 - 4B^2}} + 1}, \quad (B8a)$$

$$v_q = \frac{i}{\sqrt{2}} \sqrt{\frac{A+C}{\sqrt{(A+C)^2 - 4B^2}} - 1}. \quad (B8b)$$

The corresponding eigenvalues are

$$\omega_q^\alpha = \frac{A-C}{2} + \frac{1}{2} \sqrt{(A+C)^2 - 4B^2} \quad (B9a)$$

and

$$\omega_q^\beta = \frac{C-A}{2} + \frac{1}{2} \sqrt{(A+C)^2 - 4B^2}. \quad (B9b)$$

These are shown in Fig. 8.

APPENDIX C: ELECTRON-MAGNON COUPLING

This section considers the s - d coupling between itinerant electrons and localized spins. We consider the local coupling

$$H_{em} = J_{sd} \sum_i \mathbf{S}_i \cdot \mathbf{s}_i, \quad (C1)$$

where \mathbf{S}_i is the localized spin at site i and $\mathbf{s}_i = \sum_{\sigma, \sigma'} c_{i, \sigma}^\dagger \boldsymbol{\sigma}_{\sigma \sigma'} c_{i, \sigma'}$ is the spin of the itinerant electrons at site i . We use the Holstein-Primakoff transformation in Eq. (B2) to find

$$\begin{aligned}
 H_{em} = & J_{sd} \sum_{i,j} \{ \sqrt{2S} (a_i c_{i,\downarrow}^\dagger c_{i,\uparrow} + a_i^\dagger c_{i,\uparrow}^\dagger c_{i,\downarrow} + b_j^\dagger c_{j,\downarrow}^\dagger c_{j,\uparrow} + b_j c_{j,\uparrow}^\dagger c_{j,\downarrow}) + S[(c_{i,\uparrow}^\dagger c_{i,\uparrow} + c_{j,\downarrow}^\dagger c_{j,\downarrow}) - (c_{i,\downarrow}^\dagger c_{i,\downarrow} + c_{j,\uparrow}^\dagger c_{j,\uparrow})] \\
 & + [b_j^\dagger b_j (c_{j,\uparrow}^\dagger c_{j,\uparrow} - c_{j,\downarrow}^\dagger c_{j,\downarrow}) - a_i^\dagger a_i (c_{i,\uparrow}^\dagger c_{i,\uparrow} - c_{i,\downarrow}^\dagger c_{i,\downarrow})] \}. \quad (C2)
 \end{aligned}$$

Here, the first term describes an electron spin-flip process due to a single magnon. Because this term induces a spin flip, it is restricted to scattering between altermagnetic domains in momentum space. We account for the second term in the electron Hamiltonian in Eq. (2) because it will not induce any effective interaction but give rise to spin splitting. The third term is bilinear in magnon operators. This term is often neglected. However, for altermagnets with large spin splitting, we expect the third term to be the dominant contribution to superconductivity.

We Fourier-transform the electron-magnon terms in Eq. (C2) to find

$$\begin{aligned}
 H_{em} = & J_{sd} \sum_{k,q} \left\{ \frac{\sqrt{2S}}{\sqrt{N}} (a_q c_{a,k+q,\downarrow}^\dagger c_{a,k,\uparrow} + a_q^\dagger c_{a,k-q,\uparrow}^\dagger c_{a,k,\downarrow} + b_q^\dagger c_{b,k-q,\downarrow}^\dagger c_{b,k,\uparrow} + b_q c_{b,k+q,\uparrow}^\dagger c_{b,k,\downarrow}) \right. \\
 & \left. + \sum_{q'} \frac{1}{N} [b_{q'}^\dagger b_{q'} (c_{b,k+q-q',\uparrow}^\dagger c_{b,k,\uparrow} - c_{b,k+q-q',\downarrow}^\dagger c_{b,k,\downarrow}) - a_{q'}^\dagger a_{q'} (c_{a,k+q-q',\uparrow}^\dagger c_{a,k,\uparrow} - c_{a,k+q-q',\downarrow}^\dagger c_{a,k,\downarrow})] \right\}. \quad (C3)
 \end{aligned}$$

In terms of band electron operators and magnon operators, the interaction is $H_{em} = H_{em}^{(1)} + H_{em}^{(2)}$ with

$$\begin{aligned}
 H_{em}^{(1)} = & J_{sd} \frac{\sqrt{2S}}{\sqrt{N}} \sum_{k,q} \{ [(\Omega_{k+q,k,\downarrow}^A u_q + \Omega_{k+q,k,\downarrow}^B v_q^*) \alpha_q + (\Omega_{k+q,k,\uparrow}^A v_q + \Omega_{k+q,k,\uparrow}^B u_q^*) \beta_{-q}^\dagger] d_{k+q,\downarrow}^\dagger d_{k,\uparrow} \\
 & + [(\Omega_{k+q,k,\uparrow}^A u_q^* + \Omega_{k+q,k,\uparrow}^B v_q) \alpha_{-q}^\dagger + (\Omega_{k+q,k,\downarrow}^A v_q^* + \Omega_{k+q,k,\downarrow}^B u_q) \beta_q] d_{k+q,\uparrow}^\dagger d_{k,\downarrow} \}. \quad (C4)
 \end{aligned}$$

The second contribution is

$$H_{\text{em}}^{(2)} = \sum_{k,q,q',\sigma} \frac{J_{\text{sd}}\sigma}{N} \left[\Omega_{k+q'-q,k,\sigma,\sigma}^B (v_q^* v_{q'} \alpha_{-q} \alpha_{-q'}^\dagger + v_q^* u_{q'} \alpha_{-q} \beta_{q'} + u_q^* v_{q'} \beta_q^\dagger \alpha_{-q'}^\dagger + u_q^* u_{q'} \beta_q^\dagger \beta_{q'}) \right. \\ \left. - \Omega_{k+q'-q,k,\sigma,\sigma}^A (u_q^* u_{q'} \alpha_q^\dagger \alpha_{q'} + u_q^* v_{q'} \alpha_q^\dagger \beta_{-q'}^\dagger + v_q^* u_{q'} \beta_{-q} \alpha_{q'} + v_q^* v_{q'} \beta_{-q} \beta_{-q'}^\dagger) \right] d_{k+q'-q,\sigma}^\dagger d_{k,\sigma}. \quad (\text{C5})$$

We introduced the electron coefficients $\Omega_{k',k,\sigma',\sigma}^A \equiv q_{a,k',\sigma'}^* q_{a,k,\sigma}$ and $\Omega_{k',k,\sigma',\sigma}^B \equiv q_{b,k',\sigma'}^* q_{b,k,\sigma}$. We only consider scattering on the Fermi surface, such that the band subscript n is redundant.

APPENDIX D: EFFECTIVE INTERACTION

In this section, we derive an effective electron-electron interaction mediated by the electron-magnon coupling. We do so using a Schrieffer-Wolff transformation [54].

Let $H_0 = H_e + H_m$ and $H_1 = H_{\text{em}}$ such that we have $H = H_0 + \eta H_1$. Now, we let

$$H' = e^{-\eta S} H e^{\eta S} \quad (\text{D1})$$

and expand to find

$$H' = H_0 + \eta(H_1 + [H_0, S]) + \eta^2[H_1, S] \\ + \frac{\eta^2}{2} [[H_0, S], S] + \mathcal{O}(\eta^3). \quad (\text{D2})$$

To eliminate the linear term, we require

$$H_1 + [H_0, S] = 0. \quad (\text{D3})$$

To that end, we make the ansatz

$$S = S_1^A + S_1^B + \sum_{\sigma} (S_{2\sigma}^A + S_{2\sigma}^B), \quad (\text{D4})$$

with

$$S_1^A = J_{\text{sd}} \frac{\sqrt{2S}}{\sqrt{N}} \sum_{k,q} \\ \times \left[\Omega_{k+q,k,\downarrow,\uparrow}^A (x_{k,q} u_q \alpha_q + y_{k,q} v_q \beta_{-q}^\dagger) d_{k+q,\downarrow}^\dagger d_{k,\uparrow} \right. \\ \left. + \Omega_{k+q,k,\uparrow,\downarrow}^A (z_{k,q} u_q^* \alpha_{-q}^\dagger + w_{k,q} v_q^* \beta_q) d_{k+q,\uparrow}^\dagger d_{k,\downarrow} \right], \quad (\text{D5a})$$

$$S_1^B = J_{\text{sd}} \frac{\sqrt{2S}}{\sqrt{N}} \sum_{k,q} \\ \times \left[\Omega_{k+q,k,\downarrow,\uparrow}^B (x_{k,q} v_q^* \alpha_q + y_{k,q} u_q^* \beta_{-q}^\dagger) d_{k+q,\downarrow}^\dagger d_{k,\uparrow} \right. \\ \left. + \Omega_{k+q,k,\uparrow,\downarrow}^B (z_{k,q} v_q \alpha_{-q}^\dagger + w_{k,q} u_q \beta_q) d_{k+q,\uparrow}^\dagger d_{k,\downarrow} \right], \quad (\text{D5b})$$

$$S_{2\sigma}^A = \frac{J_{\text{sd}}}{N} \sum_{k,q,q'} -\sigma (u_q^* u_{q'} x_{k,q,q'}^{A\sigma} \alpha_q^\dagger \alpha_{q'} + u_q^* v_{q'} y_{k,q,q'}^{A\sigma} \alpha_q^\dagger \beta_{-q'}^\dagger \\ + v_q^* u_{q'} z_{k,q,q'}^{A\sigma} \beta_{-q} \alpha_{q'} + v_q^* v_{q'} w_{k,q,q'}^{A\sigma} \beta_{-q} \beta_{-q'}^\dagger) \\ \times (\Omega_{k+q-q',k,\sigma,\sigma}^A d_{k+q-q',\sigma}^\dagger d_{k,\sigma}), \quad (\text{D5c})$$

and

$$S_{2\sigma}^B = \frac{J_{\text{sd}}}{N} \sum_{k,q,q'} \sigma (v_q^* v_{q'} x_{k,q,q'}^{B\sigma} \alpha_{-q} \alpha_{-q'}^\dagger + v_q^* u_{q'} z_{k,q,q'}^{B\sigma} \alpha_{-q} \beta_{q'} \\ + u_q^* v_{q'} y_{k,q,q'}^{B\sigma} \beta_q^\dagger \alpha_{-q'}^\dagger + u_q^* u_{q'} w_{k,q,q'}^{B\sigma} \beta_q^\dagger \beta_{q'}) \\ \times (\Omega_{k+q-q',k,\sigma,\sigma}^B d_{k+q-q',\sigma}^\dagger d_{k,\sigma}). \quad (\text{D5d})$$

The condition in Eq. (D3) determines the parameters

$$x_{k,q} = \frac{1}{\varepsilon_{k,\uparrow} - \varepsilon_{k+q,\downarrow} + \omega_q^\alpha}, \quad (\text{D6a})$$

$$y_{k,q} = \frac{1}{\varepsilon_{k,\uparrow} - \varepsilon_{k+q,\downarrow} - \omega_q^\beta}, \quad (\text{D6b})$$

$$z_{k,q} = \frac{1}{\varepsilon_{k,\downarrow} - \varepsilon_{k+q,\uparrow} - \omega_q^\alpha}, \quad (\text{D6c})$$

$$w_{k,q} = \frac{1}{\varepsilon_{k,\downarrow} - \varepsilon_{k+q,\uparrow} + \omega_q^\beta}, \quad (\text{D6d})$$

and

$$x_{k,q,q'}^{A\sigma} = \frac{1}{\varepsilon_{k,\sigma} - \varepsilon_{k+q-q',\sigma} - \omega_q^\alpha + \omega_{q'}^\alpha}, \quad (\text{D7a})$$

$$y_{k,q,q'}^{A\sigma} = \frac{1}{\varepsilon_{k,\sigma} - \varepsilon_{k+q-q',\sigma} - \omega_q^\alpha - \omega_{-q'}^\beta}, \quad (\text{D7b})$$

$$z_{k,q,q'}^{A\sigma} = \frac{1}{\varepsilon_{k,\sigma} - \varepsilon_{k+q-q',\sigma} + \omega_{q'}^\alpha + \omega_{-q}^\beta}, \quad (\text{D7c})$$

$$w_{k,q,q'}^{A\sigma} = \frac{1}{\varepsilon_{k,\sigma} - \varepsilon_{k+q-q',\sigma} - \omega_{-q'}^\beta + \omega_{-q}^\beta}, \quad (\text{D7d})$$

$$x_{k,q,q'}^{B\sigma} = \frac{1}{\varepsilon_{k,\sigma} - \varepsilon_{k+q-q',\sigma} - \omega_{-q}^\alpha + \omega_{-q'}^\alpha}, \quad (\text{D8a})$$

$$y_{k,q,q'}^{B\sigma} = \frac{1}{\varepsilon_{k,\sigma} - \varepsilon_{k+q-q',\sigma} - \omega_{-q'}^\alpha - \omega_q^\beta}, \quad (\text{D8b})$$

$$z_{k,q,q'}^{B\sigma} = \frac{1}{\varepsilon_{k,\sigma} - \varepsilon_{k+q-q',\sigma} + \omega_{-q}^\alpha + \omega_{q'}^\beta}, \quad (\text{D8c})$$

$$w_{k,q,q'}^{B\sigma} = \frac{1}{\varepsilon_{k,\sigma} - \varepsilon_{k+q-q',\sigma} - \omega_q^\beta + \omega_{q'}^\beta}. \quad (\text{D8d})$$

The C_{2z} symmetry in Eq. (1a) leads to $\omega_{-q} = \omega_q$. The case $\omega_q^\alpha \neq \omega_q^\beta$ distinguishes these parameters from their analogs in conventional antiferromagnets.

The effective interaction is

$$H_{\text{eff}} = \frac{\eta^2}{2} [H_1, S]. \quad (\text{D9})$$

This commutator gives rise to several terms. We consider the quartic terms in electron operators because these terms constitute an effective electron-electron interaction. We consider scattering processes on the Fermi surface between electrons of opposite momentum only. The resulting interaction is

$$H_{e-e} = \sum_{k,k'} V_{k,k'}^{(1)} d_{k',\uparrow}^\dagger d_{-k',\downarrow}^\dagger d_{-k,\downarrow} d_{k,\uparrow} + \sum_{k,k',\sigma} V_{k,k',\sigma}^{(2)} d_{k',\sigma}^\dagger d_{-k',\sigma}^\dagger d_{-k,\sigma} d_{k,\sigma}, \quad (\text{D10})$$

with

$$\begin{aligned} V_{k,k'}^{(1)} = & \frac{J_{\text{sd}}^2 S}{N} \left[\frac{1}{\omega_{k+k'}^\alpha} (\Omega_{k',k,\uparrow,\downarrow}^A \Omega_{k',k,\uparrow,\downarrow}^A |u_{k'+k}|^2 + \Omega_{k',k,\uparrow,\downarrow}^B \Omega_{k',k,\uparrow,\downarrow}^B |v_{k'+k}|^2) \right. \\ & + \frac{1}{\omega_{k+k'}^\beta} (\Omega_{k',k,\uparrow,\downarrow}^A \Omega_{k',k,\downarrow,\uparrow}^A |v_{k'+k}|^2 + \Omega_{k',k,\uparrow,\downarrow}^B \Omega_{k',k,\downarrow,\uparrow}^B |u_{k'+k}|^2) \\ & \left. + \left(\frac{1}{\omega_{k+k'}^\alpha} + \frac{1}{\omega_{k+k'}^\beta} \right) u_{k+k'} v_{k+k'} (\Omega_{k',k,\uparrow,\downarrow}^A \Omega_{k',k,\downarrow,\uparrow}^B + \Omega_{k',k,\uparrow,\downarrow}^B \Omega_{k',k,\downarrow,\uparrow}^A) \right] \end{aligned} \quad (\text{D11})$$

and

$$V_{k,k',\sigma}^{(2)} = \frac{J_{\text{sd}}^2}{N^2} \sum_{\mathcal{Q}} (\Omega_{k',k,\sigma,\sigma}^A |v_{\frac{\mathcal{Q}-(k'-k)}{2}}| |u_{\frac{\mathcal{Q}+(k'-k)}{2}}| - \Omega_{k',k,\sigma,\sigma}^B |v_{\frac{\mathcal{Q}+(k'-k)}{2}}| |u_{\frac{\mathcal{Q}-(k'-k)}{2}}|)^2 y_{k,\frac{\mathcal{Q}+(k'-k)}{2},\frac{\mathcal{Q}-(k'-k)}{2}}^{A\sigma}. \quad (\text{D12})$$

Here, the first term is an interaction between electrons of opposite spins. This term cannot give rise to zero-momentum Cooper pairs for spin-polarized bands and, thus, not a robust superconducting state. However, the interaction in Eq. (D11) could be relevant for weak altermagnets. In this case, there is no \mathcal{PT} symmetry relating Ω^A and Ω^B as for conventional antiferromagnets. This is interesting because it could lead to an intrinsic squeezing-enhanced superconducting state. For conventional antiferromagnets, this behavior is reserved for uncompensated interfaces [52,53]. In the second term, we introduced $\mathcal{Q} = \mathbf{q} + \mathbf{q}'$. In the following, we consider potential superconductivity arising from the interaction in Eq. (D12).

APPENDIX E: SUPERCONDUCTIVITY

To estimate the critical temperature and the \mathbf{k} dependence of superconducting gap $\Delta_{k,\sigma}$, we consider the linearized gap equation

$$\Delta_{k,\sigma} = - \sum_{k'} V_{k,k',\sigma} \frac{\Delta_{k',\sigma}}{\varepsilon_{k',\sigma}} \tanh\left(\frac{\beta \varepsilon_{k',\sigma}}{2}\right). \quad (\text{E1})$$

In the continuum limit, the sum is equivalent to an integral over the Brillouin zone:

$$\Delta_{k,\sigma} = - \frac{N}{A_{\text{BZ}}} \int_{\text{BZ}} d\mathbf{k}' V_{k,k',\sigma} \frac{\Delta_{k',\sigma}}{\varepsilon_{k',\sigma}} \tanh\left(\frac{\beta \varepsilon_{k',\sigma}}{2}\right). \quad (\text{E2})$$

We now assume that the effective interaction and the gap are constant perpendicular to the Fermi surface for $|\varepsilon_k| < \omega_M$ and zero otherwise. The integral separates into one part perpendicular to the Fermi surface, and one parallel to the Fermi surface. We get

$$\begin{aligned} \Delta_{k_{\parallel},\sigma} = & - \frac{2N}{A_{\text{BZ}}} \int d\mathbf{k}'_{\parallel} \left| \frac{d\varepsilon}{d\mathbf{k}'_{\perp}} \right|^{-1} V_{k_{\parallel},k'_{\parallel},\sigma} \Delta_{k'_{\parallel},\sigma} \\ & \times \int_0^{\omega_M} d\varepsilon \frac{\tanh \beta \varepsilon / 2}{\varepsilon}. \end{aligned} \quad (\text{E3})$$

Here, ω_M is the magnon cutoff frequency. We solve for the largest eigenvalue of the equation

$$- \frac{2N}{A_{\text{BZ}}} \int d\mathbf{k}'_{\parallel} \left| \frac{d\varepsilon}{d\mathbf{k}'_{\perp}} \right|^{-1} V_{k_{\parallel},k'_{\parallel},\sigma} \Delta_{k'_{\parallel},\sigma} = \lambda \Delta_{k_{\parallel},\sigma}. \quad (\text{E4})$$

Equivalently, we have

$$- \frac{2N S_{\text{FS}}}{N_{\text{samp}} A_{\text{BZ}}} \sum_{k'_{\parallel}} \left| \frac{d\varepsilon}{d\mathbf{k}'_{\perp}} \right|^{-1} V_{k_{\parallel},k'_{\parallel},\sigma} \Delta_{k'_{\parallel},\sigma} = \lambda \Delta_{k_{\parallel},\sigma}. \quad (\text{E5})$$

The number of points N in the Brillouin zone in the numerator cancels to the denominator in $V_{k,k',\sigma}$. The area of the Brillouin zone is $A_{\text{BZ}} = \pi^2$. We sample the Fermi surface uniformly at intervals given by Eq. (A14) with a total of N_{samp} points. Now, Eq. (E5) has multiple eigenvalues. We pick out the largest one because it determines the critical temperature. The corresponding eigenvector gives the \mathbf{k} dependence of the gap $\Delta_{k,\sigma}$. We get

$$1 = \lambda_{\text{eff}} \int_0^{\omega_M} d\varepsilon \frac{\tanh \beta_c \varepsilon / 2}{\varepsilon}, \quad (\text{E6})$$

where β_c is the inverse critical temperature. The critical temperature is then related to the largest eigenvalue shown in Eq. (13).

APPENDIX F: ALTERMAGNETISM DUE TO ORDERING OF LOCAL ORBITALS

The main text considers the interplay between magnetic and nonmagnetic sites as an origin of altermagnetic properties. Anisotropic ordering of local orbitals is a different mechanism that can potentially induce an altermagnetic state.

In this section, we briefly consider the mechanism of orbital ordering as the origin of altermagnetism. To that end, we employ a tight-binding model with anisotropic hopping parameters on the lattice in Fig. 9(a).

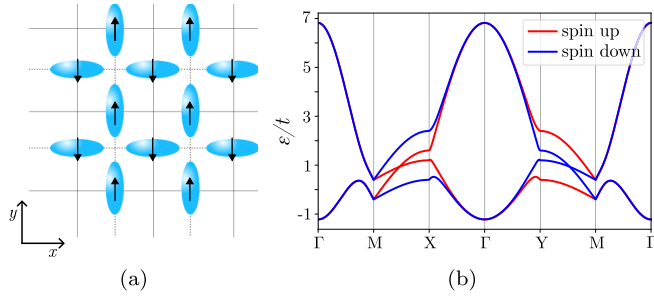


FIG. 9. (a) A two-dimensional altermagnet, with lattice sites that reflect an ordering of local atomic or molecular orbitals. The orbital ordering breaks the \mathcal{PT} symmetry to allow for altermagnetic properties. (b) The electron dispersion for the tight-binding model in Eq. (F1) with $t'_2/t = 1$, $t_2/t = 0.4$, $J_{sd}S/t = 0.4$, and $\mu/t = 0$. The bands are spin split due to the anisotropic hopping parameter.

We capture the electron properties of the orbital altermagnet through the tight-binding model

$$H_e = t_d \sum_{\langle i,j \rangle, \sigma} c_{i,\sigma}^\dagger c_{j,\sigma} + t_2 \sum_{\langle\langle i,j \rangle\rangle, \sigma} c_{i,\sigma}^\dagger c_{j,\sigma} + t'_2 \sum_{\langle\langle i,j \rangle\rangle, \sigma} c_{i,\sigma}^\dagger c_{j,\sigma} - J_{sd} \sum_{i,\sigma,\sigma'} \mathbf{S}_i \cdot \mathbf{c}_{i,\sigma}^\dagger \boldsymbol{\sigma}_{\sigma\sigma'} c_{i,\sigma'} - \mu \sum_{i,\sigma} c_{i,\sigma}^\dagger c_{i,\sigma}. \quad (\text{F1})$$

Here, t_d is the hopping parameter for diagonal hopping, and t_2 and t'_2 denote hopping along the solid and dotted lines in Fig. 9(a), respectively.

The electron eigenvalues are

$$\varepsilon_1(\mathbf{k}) = A_e + C_e - \sqrt{4B_e^2 + (C_e - A_e \pm J_{sd}S)^2} - \mu, \quad (\text{F2a})$$

$$\varepsilon_2(\mathbf{k}) = A_e + C_e + \sqrt{4B_e^2 + (C_e - A_e \pm J_{sd}S)^2} - \mu, \quad (\text{F2b})$$

where (+) is for the spin-up bands and (−) is for the spin-down bands. The parameters are defined as

$$A_e(\mathbf{k}) = t_2 \cos(k_x a) + t'_2 \cos(k_y a), \quad (\text{F3a})$$

$$B_e(\mathbf{k}) = t[\cos(k_x a + k_y a) + \cos(k_x a - k_y a)], \quad (\text{F3b})$$

$$C_e(\mathbf{k}) = t_2 \cos(k_y a) + t'_2 \cos(k_x a). \quad (\text{F3c})$$

The spin splitting can be found directly from Eq. (F2) for both bands. It is

$$\Delta_{ss}(\mathbf{k}) = \pm \left[\sqrt{4B_e^2 + (C_e - A_e + J_{sd}S)^2} - \sqrt{4B_e^2 + (C_e - A_e - J_{sd}S)^2} \right], \quad (\text{F4})$$

where we use (+) for the upper bands and (−) for the lower bands.

- [1] L. Šmejkal, J. Sinova, and T. Jungwirth, Emerging research landscape of altermagnetism, *Phys. Rev. X* **12**, 040501 (2022).
- [2] L. Šmejkal, J. Sinova, and T. Jungwirth, Beyond conventional ferromagnetism and antiferromagnetism: A phase with nonrelativistic spin and crystal rotation symmetry, *Phys. Rev. X* **12**, 031042 (2022).
- [3] R. González-Hernández, L. Šmejkal, K. Výborný, Y. Yahagi, J. Sinova, T. Jungwirth, and J. Železný, Efficient electrical spin splitter based on nonrelativistic collinear antiferromagnetism, *Phys. Rev. Lett.* **126**, 127701 (2021).
- [4] L. Šmejkal, A. B. Hellènes, R. González-Hernández, J. Sinova, and T. Jungwirth, Giant and tunneling magnetoresistance in unconventional collinear antiferromagnets with nonrelativistic spin-momentum coupling, *Phys. Rev. X* **12**, 011028 (2022).
- [5] A. Bose and D. C. Ralph, Tilted spin current generated by an antiferromagnet, *Nat. Electron.* **5**, 263 (2022).
- [6] H. Bai, L. Han, X. Y. Feng, Y. J. Zhou, R. X. Su, Q. Wang, L. Y. Liao, W. X. Zhu, X. Z. Chen, F. Pan, X. L. Fan, and C. Song, Observation of spin splitting torque in a collinear antiferromagnet RuO₂, *Phys. Rev. Lett.* **128**, 197202 (2022).
- [7] S. Karube, T. Tanaka, D. Sugawara, N. Kadoguchi, M. Kohda, and J. Nitta, Observation of spin-splitting torque in collinear antiferromagnetic RuO₂, *Phys. Rev. Lett.* **129**, 137201 (2022).
- [8] D.-F. Shao, S.-H. Zhang, M. Li, C.-B. Eom, and E. Y. Tsymlal, Spin-neutral currents for spintronics, *Nat. Commun.* **12**, 7061 (2021).
- [9] X. Zhou, W. Feng, R.-W. Zhang, L. Šmejkal, J. Sinova, Y. Mokrousov, and Y. Yao, Crystal thermal transport in altermagnetic RuO₂, [arXiv:2305.01410](https://arxiv.org/abs/2305.01410).
- [10] I. I. Mazin, Notes on altermagnetism and superconductivity, [arXiv:2203.05000](https://arxiv.org/abs/2203.05000).
- [11] D. Zhu, Z.-Y. Zhuang, Z. Wu, and Z. Yan, Topological superconductivity in two-dimensional altermagnetic metals, *Phys. Rev. B* **108**, 184505 (2023).
- [12] J. A. Ouassou, A. Brataas, and J. Linder, Josephson effect in altermagnets, *Phys. Rev. Lett.* **131**, 076003 (2023).
- [13] C. Sun, A. Brataas, and J. Linder, Andreev reflection in altermagnets, *Phys. Rev. B* **108**, 054511 (2023).
- [14] M. Papaj, Andreev reflection at altermagnet/superconductor interface, *Phys. Rev. B* **108**, L060508 (2023).
- [15] S.-B. Zhang, L.-H. Hu, and T. Neupert, Finite-momentum Cooper pairing in proximitized altermagnets, [arXiv:2302.13185](https://arxiv.org/abs/2302.13185).
- [16] S. A. A. Ghorashi, T. L. Hughes, and J. Cano, Altermagnetic routes to Majorana modes in zero net magnetization, [arXiv:2306.09413](https://arxiv.org/abs/2306.09413).
- [17] L.-D. Yuan, Z. Wang, J.-W. Luo, E. I. Rashba, and A. Zunger, Giant momentum-dependent spin splitting in centrosymmetric low-Z antiferromagnets, *Phys. Rev. B* **102**, 014422 (2020).
- [18] O. Fedchenko, J. Minar, A. Akashdeep, S. D'Souza, D. Vasilyev, O. Tkach, L. Odenbreit, Q. Nguyen, D. Kutnyakhov, N. Wind *et al.*, Observation of time-reversal symmetry breaking in the band structure of altermagnetic RuO₂, [arXiv:2306.02170](https://arxiv.org/abs/2306.02170).
- [19] K.-H. Ahn, A. Hariki, K.-W. Lee, and J. Kuneš, Antiferromagnetism in RuO₂ as *d*-wave Pomeranchuk instability, *Phys. Rev. B* **99**, 184432 (2019).
- [20] L.-D. Yuan, Z. Wang, J.-W. Luo, and A. Zunger, Prediction of low-Z collinear and noncollinear antiferromagnetic compounds

- having momentum-dependent spin splitting even without spin-orbit coupling, *Phys. Rev. Mater.* **5**, 014409 (2021).
- [21] H. Reichlová, R. L. Seeger, R. González-Hernández, I. Kounta, R. Schlitz, D. Kriegner, P. Ritzinger, M. Lammel, M. Leiviskä, V. Petříček *et al.*, Macroscopic time reversal symmetry breaking by staggered spin-momentum interaction, [arXiv:2012.15651](https://arxiv.org/abs/2012.15651).
- [22] Y. Noda, K. Ohno, and S. Nakamura, Momentum-dependent band spin splitting in semiconducting MnO₂: A density functional calculation, *Phys. Chem. Chem. Phys.* **18**, 13294 (2016).
- [23] S. Hayami, Y. Yanagi, and H. Kusunose, Momentum-dependent spin splitting by collinear antiferromagnetic ordering, *J. Phys. Soc. Jpn.* **88**, 123702 (2019).
- [24] S. A. Egorov and R. A. Evarestov, Colossal spin splitting in the monolayer of the collinear antiferromagnet MnF₂, *J. Phys. Chem. Lett.* **12**, 2363 (2021).
- [25] B. Brekke, R. Malyshev, I.-H. Svenum, S. M. Selbach, T. Tybell, C. Brüne, and A. Brataas, Low-energy properties of electrons and holes in CuFeS₂, *Phys. Rev. B* **106**, 224421 (2022).
- [26] L. Šmejkal, A. Marmodoro, K.-H. Ahn, R. Gonzalez-Hernandez, I. Turek, S. Mankovsky, H. Ebert, S. W. D'Souza, O. Šipr, J. Sinova *et al.*, Chiral magnons in altermagnetic RuO₂, [arXiv:2211.13806](https://arxiv.org/abs/2211.13806).
- [27] L. Šmejkal, R. González-Hernández, T. Jungwirth, and J. Sinova, Crystal time-reversal symmetry breaking and spontaneous Hall effect in collinear antiferromagnets, *Sci. Adv.* **6**, eaaz8809 (2020).
- [28] Z. Feng, X. Zhou, L. Šmejkal, L. Wu, Z. Zhu, H. Guo, R. González-Hernández, X. Wang, H. Yan, P. Qin *et al.*, An anomalous Hall effect in altermagnetic ruthenium dioxide, *Nat. Electron.* **5**, 735 (2022).
- [29] I. I. Mazin, K. Koepernik, M. D. Johannes, R. González-Hernández, and L. Šmejkal, Prediction of unconventional magnetism in doped FeSb₂, *Proc. Natl. Acad. Sci. USA* **118**, e2108924118 (2021).
- [30] M. Naka, Y. Motome, and H. Seo, Perovskite as a spin current generator, *Phys. Rev. B* **103**, 125114 (2021).
- [31] S. López-Moreno, A. Romero, J. Mejía-López, and A. Muñoz, First-principles study of pressure-induced structural phase transitions in MnF₂, *Phys. Chem. Chem. Phys.* **18**, 33250 (2016).
- [32] T. Okugawa, K. Ohno, Y. Noda, and S. Nakamura, Weakly spin-dependent band structures of antiferromagnetic perovskite LaMO₃ (M = Cr, Mn, Fe), *J. Phys.: Condens. Matter* **30**, 075502 (2018).
- [33] Y. Guo, H. Liu, O. Janson, I. C. Fulga, J. van den Brink, and J. I. Facio, Spin-split collinear antiferromagnets: A large-scale ab-initio study, *Mater. Today Phys.* **32**, 100991 (2023).
- [34] H.-Y. Ma, M. Hu, N. Li, J. Liu, W. Yao, J.-F. Jia, and J. Liu, Multifunctional antiferromagnetic materials with giant piezomagnetism and noncollinear spin current, *Nat. Commun.* **12**, 2846 (2021).
- [35] K. S. Burch, D. Mandrus, and J.-G. Park, Magnetism in two-dimensional van der Waals materials, *Nature (London)* **563**, 47 (2018).
- [36] B. Huang, G. Clark, E. Navarro-Moratalla, D. R. Klein, R. Cheng, K. L. Seyler, D. Zhong, E. Schmidgall, M. A. McGuire, D. H. Cobden *et al.*, Layer-dependent ferromagnetism in a van der Waals crystal down to the monolayer limit, *Nature (London)* **546**, 270 (2017).
- [37] A. K. Geim and I. V. Grigorieva, Van der Waals heterostructures, *Nature (London)* **499**, 419 (2013).
- [38] M. Naka, S. Hayami, H. Kusunose, Y. Yanagi, Y. Motome, and H. Seo, Spin current generation in organic antiferromagnets, *Nat. Commun.* **10**, 4305 (2019).
- [39] P. Liu, J. Li, J. Han, X. Wan, and Q. Liu, Spin-group symmetry in magnetic materials with negligible spin-orbit coupling, *Phys. Rev. X* **12**, 021016 (2022).
- [40] S. Bhowal and N. A. Spaldin, Magnetic octupoles as the order parameter for unconventional antiferromagnetism, [arXiv:2212.03756](https://arxiv.org/abs/2212.03756).
- [41] P. A. McClarty and J. G. Rau, Landau theory of altermagnetism, [arXiv:2308.04484](https://arxiv.org/abs/2308.04484).
- [42] J. Linder and J. W. Robinson, Superconducting spintronics, *Nat. Phys.* **11**, 307 (2015).
- [43] F. S. Bergeret, A. F. Volkov, and K. B. Efetov, Odd triplet superconductivity and related phenomena in superconductor-ferromagnet structures, *Rev. Mod. Phys.* **77**, 1321 (2005).
- [44] J. Robinson, J. Witt, and M. Blamire, Controlled injection of spin-triplet supercurrents into a strong ferromagnet, *Science* **329**, 59 (2010).
- [45] M. Eschrig, Spin-polarized supercurrents for spintronics: A review of current progress, *Rep. Prog. Phys.* **78**, 104501 (2015).
- [46] J. G. Bednorz and K. A. Müller, Possible high T_c superconductivity in the Ba-La-Cu-O system, *Z. Phys. B* **64**, 189 (1986).
- [47] S. Chakravarty, B. I. Halperin, and D. R. Nelson, Two-dimensional quantum Heisenberg antiferromagnet at low temperatures, *Phys. Rev. B* **39**, 2344 (1989).
- [48] M. Kargarian, D. K. Efimkin, and V. Galitski, Amperean pairing at the surface of topological insulators, *Phys. Rev. Lett.* **117**, 076806 (2016).
- [49] N. Rohling, E. L. Fjærbu, and A. Brataas, Superconductivity induced by interfacial coupling to magnons, *Phys. Rev. B* **97**, 115401 (2018).
- [50] E. L. Fjærbu, N. Rohling, and A. Brataas, Superconductivity at metal-antiferromagnetic insulator interfaces, *Phys. Rev. B* **100**, 125432 (2019).
- [51] K. Mæland and A. Sudbø, Topological superconductivity mediated by skyrmionic magnons, *Phys. Rev. Lett.* **130**, 156002 (2023).
- [52] E. Erlandsen, A. Kamra, A. Brataas, and A. Sudbø, Enhancement of superconductivity mediated by antiferromagnetic squeezed magnons, *Phys. Rev. B* **100**, 100503(R) (2019).
- [53] E. Thingstad, E. Erlandsen, and A. Sudbø, Eliashberg study of superconductivity induced by interfacial coupling to antiferromagnets, *Phys. Rev. B* **104**, 014508 (2021).
- [54] J. R. Schrieffer and P. A. Wolff, Relation between the Anderson and Kondo Hamiltonians, *Phys. Rev.* **149**, 491 (1966).
- [55] J. Bardeen, L. N. Cooper, and J. R. Schrieffer, Theory of superconductivity, *Phys. Rev.* **108**, 1175 (1957).
- [56] M. Sigrist and K. Ueda, Phenomenological theory of unconventional superconductivity, *Rev. Mod. Phys.* **63**, 239 (1991).
- [57] Q. Cui, B. Zeng, P. Cui, T. Yu, and H. Yang, Efficient spin Seebeck and spin Nernst effects of magnons in altermagnets, *Phys. Rev. B* **108**, L180401 (2023).